J Mater Sci (2007) 42:1360–1368
DOI 10.1007/s10853-006-1216-z

Mechanical improvement of hydroxyapatite by TiO_x nanoparticles deposition

J. R. Díaz-Estrada · E. Camps · L. Escobar-Alarcón · J. A. Ascencio

Received: 10 October 2004 / Accepted: 6 February 2006 / Published online: 1 December 2006

Abstract Deposition of Ti was carried out by laser ablation onto hydroxyapatite porous discs in an Ar atmosphere. Ti nanoparticles were deposited onto HAp surface in order to modify its roughness and morphology as it is observed by scanning electron microscopy (SEM) and scanning probe microscopy (SPM). A homogeneous distribution of Ti over the disc surface was corroborated by elemental mapping. A comparison of the hydroxyapatite hardness before and after deposition was performed using SPM nanoindentation. Transmission Electron Microscopy (TEM) showed that the Ti nanoparticles obtained were covered by an oxygen shell. It is shown that surface modifications of the covered HAp by Ti result in better mechanical properties, reducing the possible damage to the HAp ceramic by friction or impacts as it often happens in meniscus, bone junctions and the inclusion of prosthesis for human treatments.

J. R. Díaz-Estrada · J. A. Ascencio
Facultad de Química, Universidad Autónoma del Estado de México, Colon y Tollocan, Toluca, Edo. de México, Mexico

J. R. Díaz-Estrada · E. Camps · L. Escobar-Alarcón
Departamento de Física, Instituto Nacional de Investigaciones Nucleares, Apartado postal 18-1027, Mexico, DF 11801, Mexico

J. A. Ascencio (✉)
Instituto Mexicano del Petróleo, Eje Central Lázaro Cárdenas 152, Mexico, D.F 07730, Mexico
e-mail: ascencio@imp.mx

Introduction

Hydroxyapatite (HAp) $Ca_{10}(PO_4)_6(OH)_2$ with an atom ratio Ca/P = 1.67 is the ideal phase of mineral apatite, which can be found on bones and teeth. Several studies have been focused on its synthesis; characterization and processing for specific purposes such as bone fillers, bone augmentation and regeneration among others. While many works have been developed with the idea of forming HAp similar materials to be used as prosthesis [1–3], there are also multiple reports about the structure [4–6] and the interaction of hydroxyapatite with other calcium phosphates [6], and metallic materials [7] in order to identify the best conditions to use materials and shapes for human prosthesis [3, 5–7]. In general the biomaterials development has become quite important and the use of new materials and new development methods open excellent perspectives to apply prosthesis with less repercussions to the bones and human body, helping to a faster and better recovering of health [8, 9] and improving the performance of the prostheses under the particular conditions of human body.

The use of nanometric particles is well established for materials improvement, in order to produce better optical [10], electrical [11], or mechanical [12–15] among other properties. Particularly the use of nanoparticles and inorganic fullerene-like nanostructures have demonstrated to have excellent tribological properties [14, 15], so the use of these materials on the HAp surface is considered to improve the mechanical properties; which can be used in human prosthesis, as in knees and mandible junction cases, where the continuous movements induce several complication in the boundary. Nanostructured materials can be

synthesized by chemical and physical methods; particularly the laser ablation has been recognized as an important tool to generate nanoparticles [16–18], and thin films [19–21]. By varying the experimental conditions (energy density or working pressure) it is possible to control the size of the deposited nanoparticles [22].

The use of nanostructured biocompatible materials like Ti, as lubricant on the prosthesis will open a wide scope of applications for sport medicine and prosthesis design, considering that the two main problems in the inclusion of new materials for prosthesis are compatibility and mechanical interaction with its surrounding environment. In this work we study the HAp surface, the coating process with Ti nanoparticles by laser ablation, and on the study of the properties change of the coated HAp material. Scanning electron microscopy (SEM), energy dispersive spectroscopy (EDS), X-ray diffraction (XRD) and scanning probe microscopy (SPM) including nanoindentation were the techniques used for the analysis of the obtained material.

Experimental procedure

Experimental setup

The pulsed laser deposition system used in these experiments was developed in our laboratory and is described in detail elsewhere [23]. The system consists of a stainless steel vacuum chamber evacuated by a diffusion pump. A pirani and a cold cathode gauge were used to measure the total pressure of the vacuum chamber. The laser used in these experiments was a Nd:YAG laser (1064 nm) using energy densities close to 9.4 and 7.4 J/cm^2 with 28 ns pulse duration at a repetition rate of 10 Hz. The laser beam was focused with a spherical lens of 250 mm focal length; its incidence angle was 65°. The target and substrate holder were set parallel and the distance between them was fixed at 50 mm. The deposition chamber was initially evacuated to pressures in the 10^{-6} Torr range and then filled with high purity argon gas (99.999%) at different working pressures ranging from 0.01 to 0.2 Torr. The argon pressure was controlled by a needle valve. The target was rotated with an electric motor to avoid depletion of material at any given spot.

Substrate and target preparation

Commercial Ti pellet (Kurt J. Lesker 99.999 % pure) was used as target. The substrates used were HAp discs prepared under pressure by the method described in [24] and modified for this purpose. Before deposition the HAp discs were cleaned using pressurized air.

Nanoparticles characterization

Characterization of deposits was carried out using a Scanning Electron Microscope Philips XL-30 ESEM provided with an EDAX detector to perform EDS analysis and to verify that the atom ratio Ca/P remains unaltered after deposition; elemental mapping was used to determine the distribution of Ti over the HAp disc surface after deposition. Substrates were not coated with carbon or gold when they were analyzed by SEM. TEM analyses were made using a JEOL 2010 microscope operating at 200 keV, with an energy filter for elemental composition analysis by Gatan, and an internal CCD for direct processing and resolution improvement up to 0.21 nm. XRD analyses were carried out with a D-5000 Siemens diffractometer. X-ray diffraction analyses were performed in order to determine the corresponding crystalline phases before and after depositions onto the substrates. A more detailed morphology study was carried out using a Nanoscope IV Atomic Force Microscope by Digital Instruments using contact mode, tapping mode and nanoindentation mode. Tapping mode was employed for a better resolution of the nanoparticles deposited over the HAp and to observe the homogeneity of these depositions. Contact mode was used to evaluate friction and adhesion of particles to the HAp surface. Hardness results were obtained with the AFM nanoindentation mode using a Berkovich diamond indenter with face angle of 60°.

Results and discussion

The most important characteristics of HAp as a substrate are: surface morphology, the ratio Ca/P and crystalline structure, which are directly related to the porosity and mechanical properties [5]. The first one was evaluated with SEM and AFM, the rest of them with EDS and XRD analyses. Figure 1a shows a SEM micrograph of the HAp surface disc, where two main grain sizes can be identified. Big grains are sized around 20 μm, while the smallest particles are around 1 μm. It is worth noting that porosity was induced during the processing of disks. Pores observed in Fig. 1a are approximately 8 μm in diameter. A more detailed image is shown in Fig. 1b, where a higher magnification micrograph is shown. It can be seen that the observed grains are formed by particles and fibers

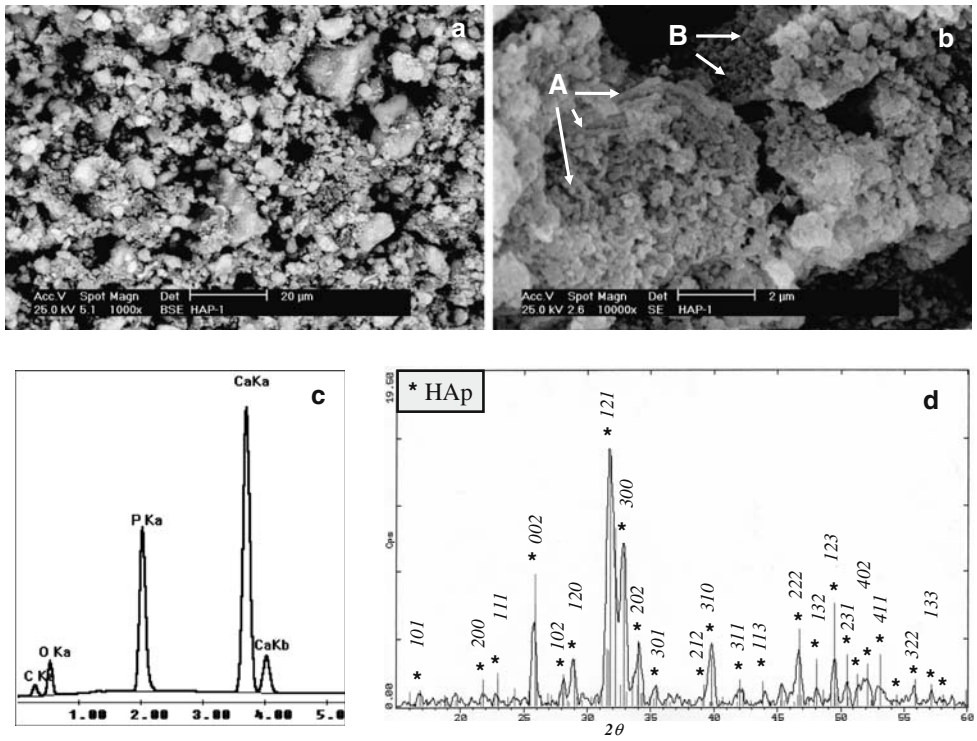

Fig. 1 HAp SEM micrographs (a) 1,000× and (b) 10,000×, the corresponding (c) EDS, and (d) X-ray diffraction patterns

(A in Fig. 1b) of 150 nm in radius and 1 μm in length (fibers are parallel to the electron beam axis and the profile must be identified); there are also grains with a porosity in the order of 100 nm also (B in Fig. 1b). The corresponding EDS pattern is shown in Fig. 1c, where the main peak is from the Ca atoms, while the P and O signals are also evidenced as it was expected for the HAp. The crystal structure is characterized by the XRD pattern (Fig. 1d), which match with the hexagonal crystal lattice of HAp[25]. These shapes and structure have been reported previously for HAp as produced by several mechanisms of crystal growing, which are dominated by the crystal habit [4, 5, 26].

In order to study the morphology regularity and structural profiles in a lower scale, we made an analysis of AFM tapping mode for the HAp bare samples. Figure 2a–c show the morphology, phase and profile section for one of the grains identified in the SEM micrographs, it is clear that these grains are formed by small clusters of around 70 nm in average. The profile indicates the formation of small grains with height of just 160 nm as observed in the *i* curve; while in *ii* curve two grains of height up to 378 nm and 469 nm are detected. The phase image denotes a high regularity in the interaction of the tip with the sample; this is related to a homogeneous composition. The 3D image from an 800 nm × 800 nm scanned area (Fig. 2d) allows identifying the fibers observed by SEM in Fig. 1b. The grains are formed by the aggregation of smaller clusters producing elongated forms, which are usually related to small range HAp crystal growing, based in its crystalline lattice [5, 25]. It must be noticed that the height scale is 170 nm, so the material topography denotes the porosity and morphology of the HAp. The faceted and angular shapes domain the surface of the sample as it was expected for this ceramic, where the formation of fibers are common and the porosity implies a topography as the one observed here.

From the above obtained results, it is seen that the HAp produced in this work has a commonly identified structure in multiple reports [3–6, 26]. In our case this material was used as the substrate for the deposition of the nanostructured Ti material. The experimental conditions variation allows obtaining the nanoparticles with different size and distribution, which will be discussed later below. The HAp substrate covered with the Ti oxide material was analyzed by SEM, both surface morphology and elemental composition distributions on the substrate by elemental mapping based on the characteristic X-ray were studied. In Fig. 3a, a wide scope of the HAp surface with Ti coating is observed, where it is clear how the surface morphology is mainly determined by the substrate, but with a reduced grain contrast that was observed in the case of bare HAp. A higher magnification image (Fig. 3b), demonstrates the homogeneous conformation of the

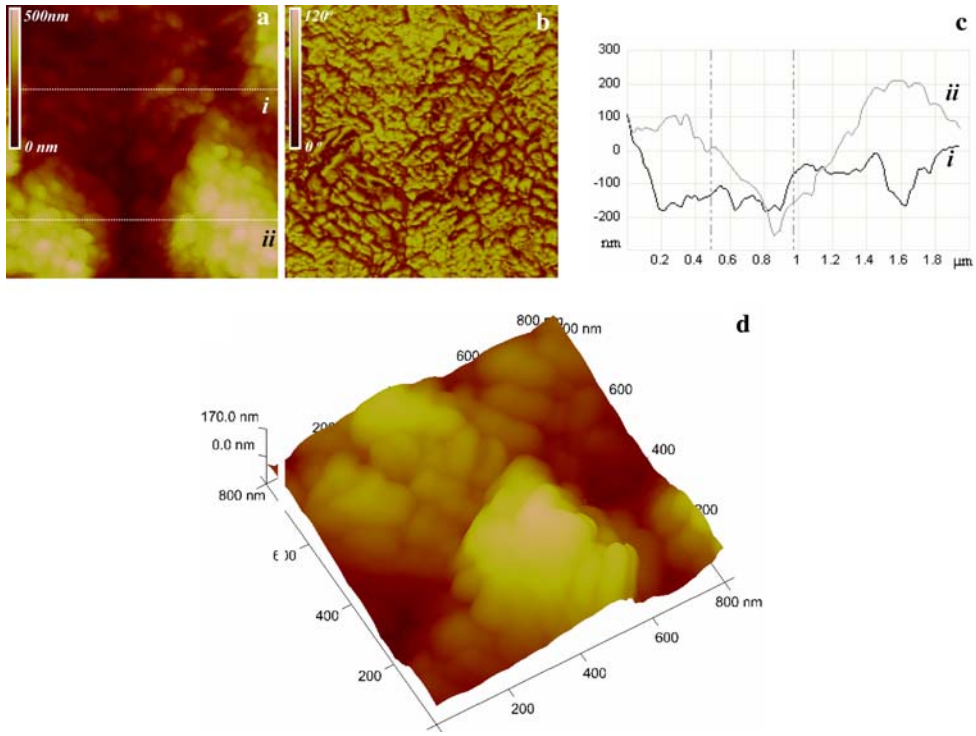

Fig. 2 AFM analysis of the HAP bare samples. Images of a 2 µm × 2 µm scan for (a) height and (b) phase with (c) its corresponding profile section for the i and ii doted lines, and (d) a higher magnification 3D image

deposit by small clusters of around 100 nm, which are aggregated on the HAp substrate. The sample with deposited nanostructures was also studied by EDS in order to determine the distribution of the material. A micrograph of the surface (Fig. 3c) and corresponding elemental mapping of Ti and O are shown. It is clear that the elemental mapping composition denotes a homogeneous distribution of the Ti and O on the surface.

Four main deposition conditions were found as the best to produce a homogeneous coating. For samples made under that conditions AFM analyses were carried out for them, in order to determine the size distribution of the deposited particles and the produced morphology in the surface. The four main conditions were obtained from two values of the working pressure $P = 0.200$ and 0.075 Torr, and two values of the energy density delivered onto

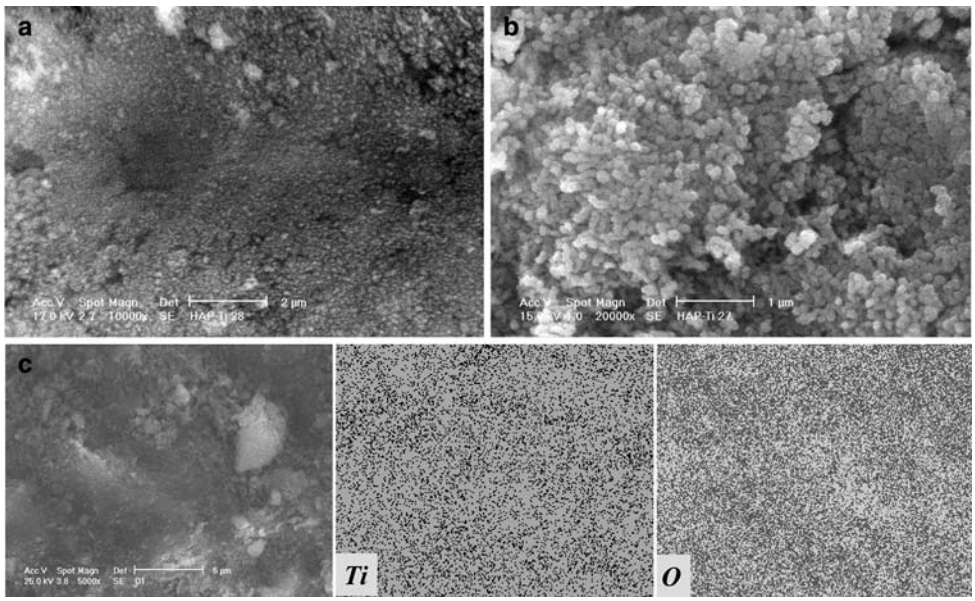

Fig. 3 SEM micrographs of TiO_x deposit on the HAp substrate at (a) 10,000× and (b) 20,000×, and (c) an image at 5,000× with its corresponding elemental maps for Ti and O

the target by the laser (i.e, fluence) $F = 9.4$ and 7.4 J/cm^2, the samples shown in Figure 4 were prepared in these conditions. In the four cases aggregates covered by smaller particles are observed, however there are several significant differences between them.

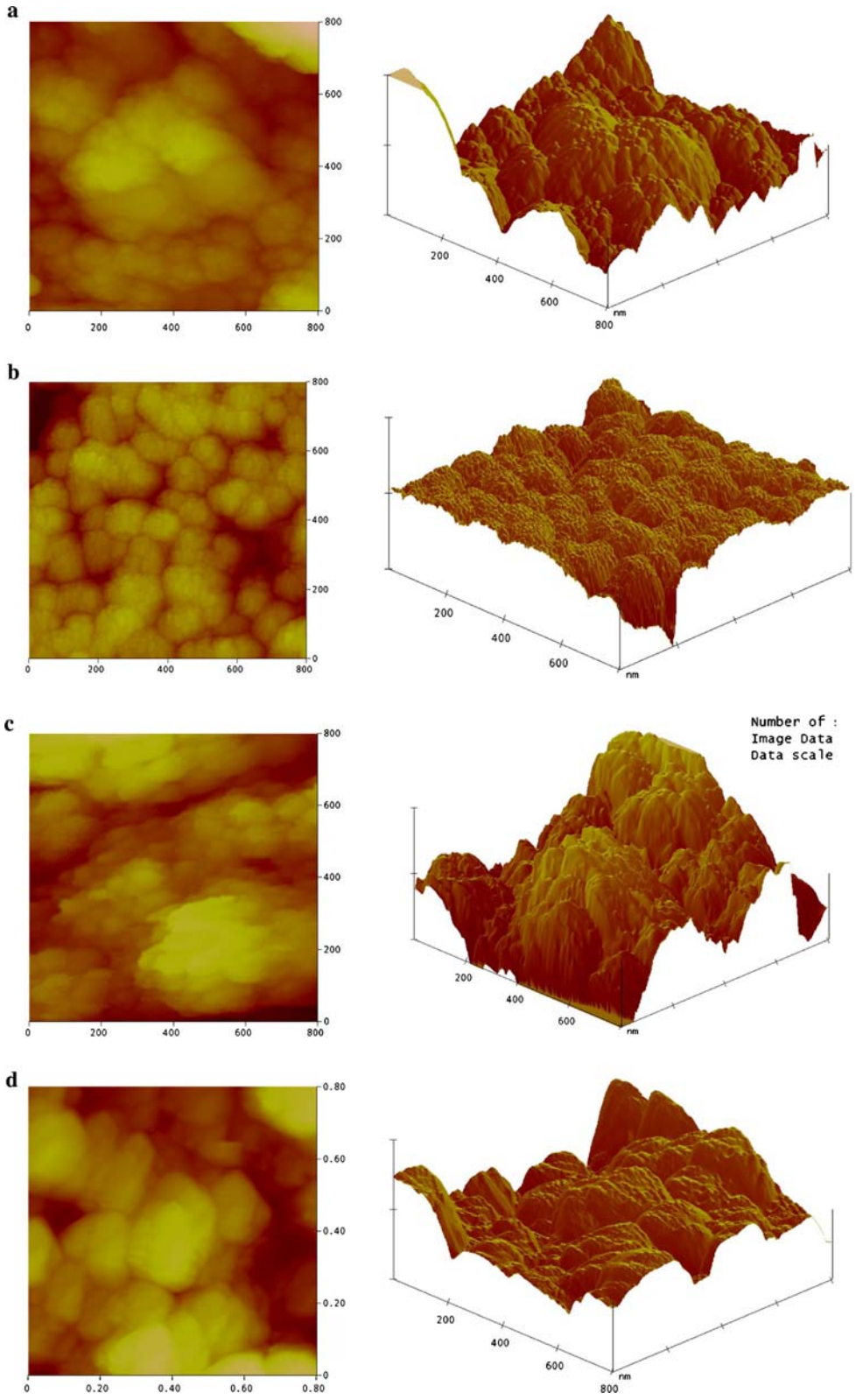

Fig. 4 Tapping mode study of height and 3D images for samples prepared during 10 min and: (a) $P = 0.2$ Torr, $F = 9.4$ J/cm^2; (b) $P = 0.2$ Torr, $F = 7.4$ J/cm^2; (c) $P = 0.075$ Torr, $F = 7.4$ J/cm^2; (d) $P = 0.075$ Torr, $F = 9.4$ J/cm^2

Figure 4a shows a sample produced at $P = 0.2$ Torr and $F = 9.4$ J/cm^2 with particle size ranging from 20 to 60 nm covering the HAp, while the sample in Fig. 4b deposited at $P = 0.2$ Torr and $F = 7.4$ J/cm^2, shows bigger clusters with sizes from 30 to 70 nm. Figures 4c and d show pictures of samples obtained at $P = 0.075$ Torr and two values of fluence, 7.4 J/cm^2 (Fig. 4c) and 9.4 J/cm^2 (Fig. 4d). For the case of Fig. 4c nanoparticles with sizes from 7 to 25 nm cover the HAp producing a smoother surface, and finally Fig. 4d shows the HAp surface covered by particles with sizes ranging from 10 to 150 nm. From these experiments we determined the best conditions to produce the smallest and most homogeneous particle distribution, which in this case correspond to the sample observed in Fig. 4c.

The size of the formed nanoparticles can be related to the working pressure used. Our results indicate that for low pressure generated a low agglomeration of particles; this can be due to the lack of interaction between the plasma species because of the large mean free path. At higher pressures the plume species undergo more collisions and the clustering between species is favored. Then the tendency observed in this work shows that the nanoparticle and cluster size increases with the pressure at moderate fluences. When the fluence is increased a higher dispersion is observed due to an increase in the plasma density near the target and to a higher energy of the particles which reach the substrate. Phase signal shows a homogeneous phase distribution of deposited material. Friction signal shows how difficult is for the tip to scan the surface, as it can be seen on the image, at that places where there are no Ti particles there exists a higher friction than in the rest of the surface. Figure 4a and b show multiple fringes produced during the microscope tip scanning on the surface, indicating a difficulty to obtain a good image due to a bad adhesion of the particles to the substrate. These images can be enhanced using the tapping mode of the microscope, as in this mode the interaction time of the tip and the substrate is reduced.

In order to study the shape and structure of single Ti nanoparticles, they were analyzed by transmission electron microscopy. The analysis showed that the nanoparticles are composed of small aggregates of Ti atoms surrounded by a titanium oxide shell. In Fig. 5, a small nanoparticle can be observed in a high resolution

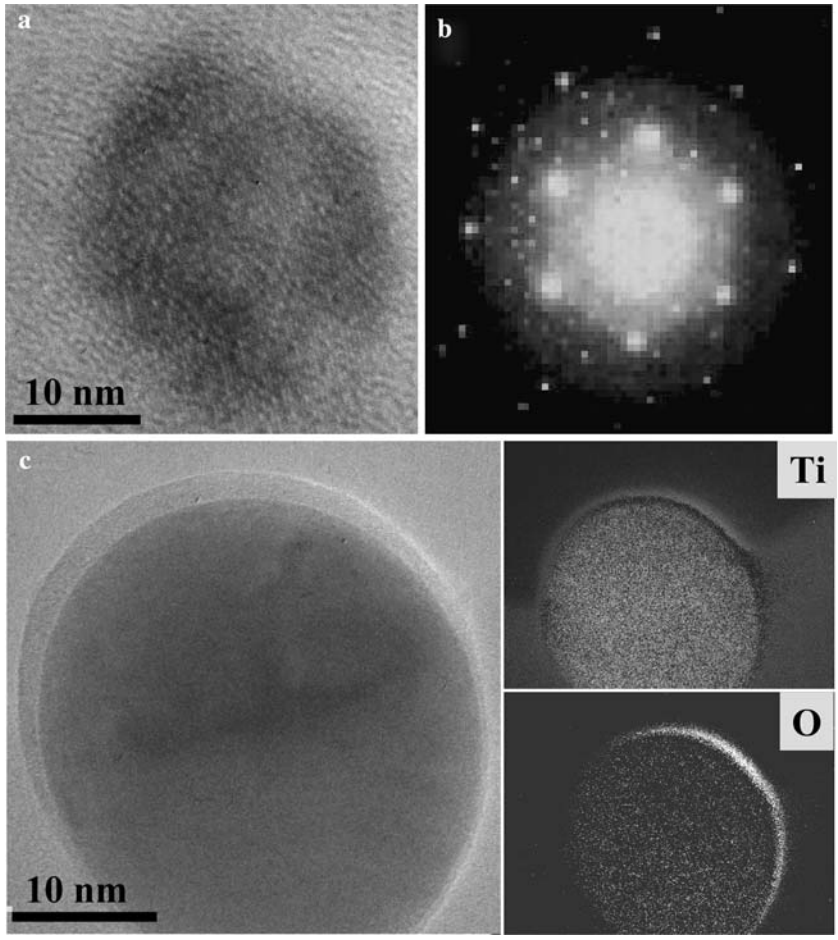

Fig. 5 TEM study of produced Ti-core/O-shell nanoparticles. (a) HREM image, (b) EDP, (c) bright field image with elemental maps for Ti and O and (d) a proposed model with its corresponding simulated HREM image and EDP

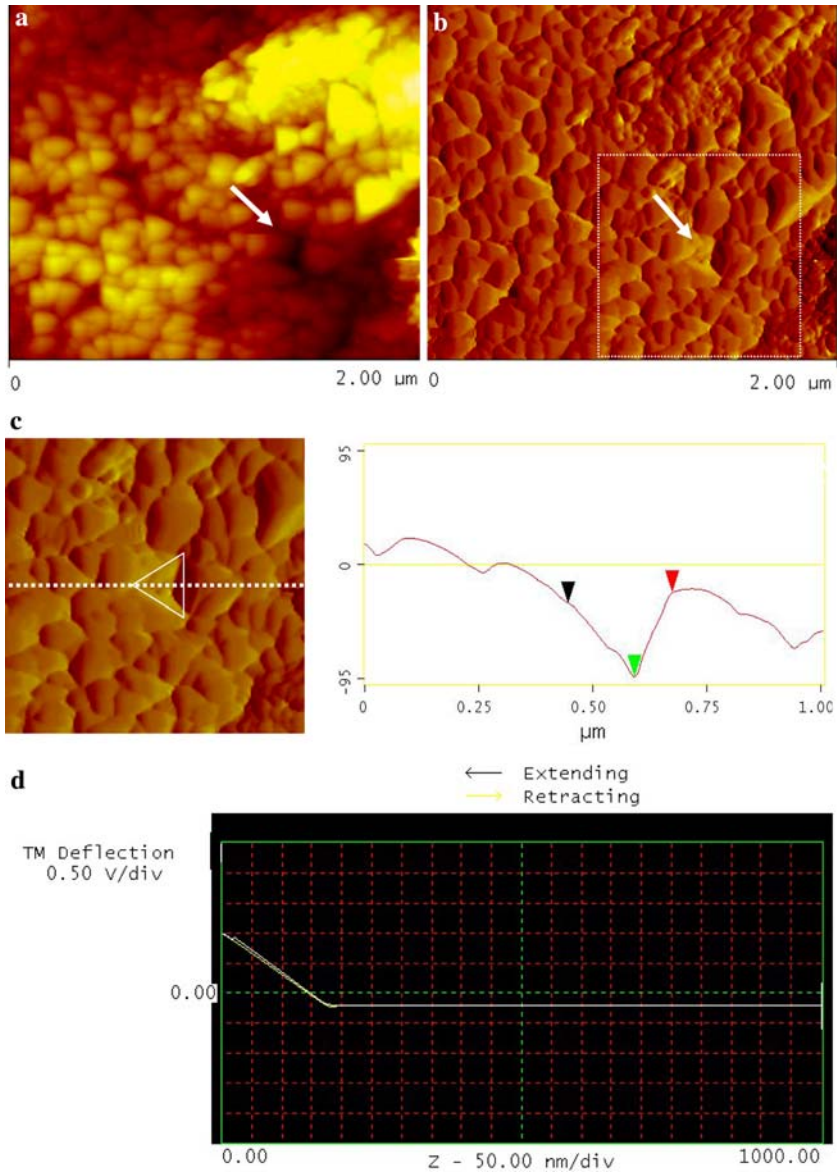

Fig. 6 Nanoidentation analysis of HAp covered with TiO_x. (a) Corresponding height with the (b) friction images besides (c) a section profile and (d) the obtained plot for the nanoindentation evaluation

image (Fig. 5a) with its corresponding electron diffraction pattern (Fig. 5b) denoting a hexagonal array of atoms that matches in symmetry and distances on the FFT to the bulk crystal symmetry. Using bright field contrast for a particle with diameter of 35 nm (Fig. 5c) we can observe that the core is composed by a heavier element while the shell is based in small atomic number (Z) atoms. Besides with help of high angle annular dark field (HAADF) signal (that is based on the inelastic scattering, related to Z^2 and consequently to the elemental composition [27]) and using energy filtering we identified the regions rich in Ti and O respectively. The analysis allows determining that even when the Ti is present in whole particle, oxygen is found just in the shell. These results determine an oxidation process of the nanoparticles surfaces; however the main structure is based on the Ti bulk symmetry.

The TEM analysis allows determining the formation of nanoparticles around 30 nm, where the core-shell structure has a hexagonal atomistic symmetry and a rounded profile as it was expected and considered from the previous methods and it must be on the HAp sample as a fine powder coating.

The previous measured characteristics of the coated HAp are reflected on the material properties and, in this particular case, on the mechanical properties obtained and evaluated by nanoidentación using the SPM (Fig. 6) [28]. A diamond tip is used to produce a mark on the sample surface and the forces required to

produce this mark are measured. From these measurements the differences between the deflection of the tip in the extending and retracting paths are evaluated. Figure 6 shows an example of the study for a sample deposited at a pressure of 0.075 Torr, and a fluence of 7.4 J/cm^2 during 10 min. In Fig. 6a, a height image of the zone where the indentation was made is observed besides the friction image (Fig. 6b), where the shape of the indentation is clear but also it is evident the displacement of material during the process (see the marked zones with arrows), which must be considered for an evaluation of the application perspectives of this material. From Fig. 6c, it is possible to observe the profile of the analyzed section obtained from the indentation zone. It is clear the flat shape of the produced hole, but it can also be observed the smoothness of the surface that must reduce the damages to the HAp matrix. Furthermore, Fig. 6d shows a deflection plot, where a small shift of the extending and retracting paths can be observed. It must be noticed that the surface morphology resolution is much lower than in the previous images, because we used the diamond tip for this study, which is much bigger than the one used for tapping. The evaluation of hardness is involved to the response of the tip when it is pushed to the surface of the material as it can be obtained from the applied force and the height of the produced hole.

The material improvement is evidenced from its smooth shape but also from the nanoindentation plots. In fact we can recognize four main coatings on the HAp, which depend on the synthesis conditions producing different nanoparticle sizes which affect the mechanical properties of the HAp. In our case the goal is to reduce the effects of solid–solid interaction between two pieces of bone or between a bone with prosthesis, so the lubrication induced by the nanoparticles must reduce the local effects of pressures or impacts. Evaluation by means of the nanoindentation method allows us understanding the differences of deformation and fracture possible risks. In fact, the parameter of rigidity of a sample is inversely proportional to the local hardness, which represents the obstacle to insert an intruding object in the surface of the HAp producing possible damages to the material.

In order to analyze the effect of the coating on the hardness of the samples, the nanoindentation method was used in different zones of the samples, and a resume of average values is shown in Table 1, where the hardness is evaluated for different samples. The values are calculated as the Martnes or universal hardness for the conditions of a Berkovich indentator that is based in the formula

Table 1 Hardness average values for the different samples of HAp and TiO_x deposits on HAp

Material	Fluency (J/cm^2)	Pressure (Torr)	Hardness (MPa)
HAp (bare)			90.1
HAp with TiO_x deposit	9.4	0.075	88.8
		0.200	57.0
	7.4	0.075	40.0
		0.200	37.1

$$H_M = \frac{F_A}{A_5(h)} = \frac{F_A}{26.44h^2},$$

where F_A corresponds to the applied force, and h to the produced indentation depth, while A_5 is the projected area of the indentation zone [29].

It can be noticed that the hardness is significantly lower for the HAp with the TiO_x deposit than without it, which implies a higher softness of the surface and in consequence the force to produce permanent deformation on the HAp surface is increased.

Conclusions

With a laser ablation method we can conclude that TiO_x nanoparticles are produced in sizes from 8 to 70 nm based in the atmosphere and energy (fluence) conditions. The optimum parameters for the present work turned out to be a fluence of 7.4 J/cm^2 and a pressure of 0.075 Torr that produced small particles and high homogeneity. The nanoparticles were deposited on the irregular surface of HAp producing a smoother morphology and covering totally the ceramic.

The characterization methods allowed determining a structure of Ti core cluster with a thin titanium oxide shell for the particles pasivating the surface and generating spherical shapes in the material. The coating on the HAp surface reduced up to 62% the hardness of the material, and in consequence the damage produced on the substrate is reduced significantly. Using AFM analysis the evidences of friction images determined the lubricant effect of the TiO_x particles, which generate a layer of around 80 nm improving the tribological capacity of the HAp. A potential application for this material is the substitution of meniscus but also, because of the nanoparticles size the tribological properties of the obtained material must be much higher and the applications as a lubricant between bones and prosthesis becomes especially important.

This work opens a wide scope of application for small particles as coating for prosthesis and for direct application on the surface of bones in order to reduce the friction of the pieces and the corresponding damages to the osseous structure in the human body. It can be used also in the inclusion of metallic prosthesis which uses to be the critical point to consider for reconstruction surgery and damage fixing.

Acknowledgements The authors are indebt to L. Carapia, because his technical help in the SEM study. And particularly thank the support of G. Canizal and L. Martínez. for AFM analysis. Especially we want to thank the collaboration of P. Santiago for TEM analysis.

References

1. Chern-Lin JH, Chen KS, Ju CP (1995) Mat Chem Phys 41:282
2. Kurashina K, Kurita M, Hirano HM, de Bliek JMA, Klein CAT, de Groot K (1995) J Mat Sci Mat Med 6:340
3. Rodríguez-Lugo V, Ascencio JA, Angeles-Chavez C, Camacho-Bragado A, Castaño VM (2001) Mat Techn 16:97
4. Zhang LJ, Feng XS, Liu HG, Qian DJ, Zhang L, Yu XL, Cui FZ (2004) Mat Lett 58:719
5. Ascencio JA, Rodriguez-Lugo V, Angeles C, Santamaria T, Castano VM (2002) Comp Mat Sci 25:413
6. Fernández ME, Zorrilla-Cangas C, García-García R, Ascencio JA, Reyes-Gasga J (2003) Acta Cryst B59:175
7. Souto RM, Laz MM, Reis RL (2003) Biomaterials 24:4213
8. Fricain JC, Granja PL, Barbosa MA, de Jéso B, Barthe N, Baquey C (2002) Biomaterials 23:971
9. Ignjatović N, Savić V, Najman S, Plavšić M, Uskoković D (2001) Biomaterials 22:571
10. Li J, Chen Ch, Zhao J, Zhu H, Orthman J (2002) App Cat B: Env 37:331
11. Meng WJ, Titsworth RC, Rehn LE (2000) Thin Solid Films 377–378:222
12. Gittins DI, Bethell D, Schiffrin DJ, Nichols RJ (2000) Nature 408:67
13. Ascencio JA, Perez-Alvarez M, Molina LM, Santiago P, José-Yacaman M (2003) Surf Sci 526:243
14. Rapoport L, Bilik Y, Feldman Y, Homyonfer M, Cohen SR, Tenne R (1997) Nature 387:791
15. Chowalla M, Amaratunga GAJ (2000) Nature 407:164
16. Ullmann M, Friedlander SK, Schmidt-Ott A (2002) J Nanop Res 4:499
17. Makino T, Susuki N, Yamada Y, Yoshida T, Seto T, Aya N (1999) App Phys A 69:S243
18. Koshizaki N, Narazaki A, Sasaki T (2002) App Surf Sci 197–198:624
19. Gamaly EG, Rode AV, Perrone A, Zocco A (2001) App Phys A 73:143
20. Fu ZW, Zhou MF, Qin QZ (1997) App Phys A 65:445
21. Doeswijk LM, Rijnders G, Blank DHA (2004) App Phys A 78:263
22. Nichols WT, Malyavanatham G, Henneke DE, Brock JR, Becker MF, Keto1 JW, Glicksman HD (2000) J Nanop Res 2:141
23. Escobar-Alarcón L, Villagran M, Haro-Poniatowski E, Alonso JC, Fernández-Guasti M, Camps E (1999) App Phys A 69:s583
24. Díaz-Estrada JR (1998) *Preparación y caracterización de esferas de hidroxiapatita para globo ocular*, Mexico, Chemical Engineering Thesis; U.N.A.M
25. Park JB, (1984) Biomaterials science and engineering. New York, Plenum Press
26. Liu Y, Sethuraman G, Wu W, Nancollas GH, Grynpas M (1997) J Coll Interf Sci 186:102
27. Bischel MS, Vanlandingham MR, Eduljee RF, Gillespie JW, Schultz JM (2000) J Mat Sci 35:221
28. CSM Instruments. Advanced mechanical surface testing; overview of mechanical testing standards, (Application Bulletin 18, 2002)